NUMERICAL SIMULATION OF TITANIUM ALLOY DRY MACHINING WITH A STRAIN SOFTENING CONSTITUTIVE LAW

Madalina Calamaz[1], Dominique Coupard[1], and Frank Girot[1,2]

[1] *Laboratoire Matériaux Endommagement Fiabilité Ingénierie des Procédés (LAMEFIP), Arts et Métiers ParisTech, CER de Bordeaux, Esplanade des Arts et Métiers, Talence, France*

[2] *Department of Mechanical Engineering, ETSIB, University of the Basque Country, Alameda de Urquijo s/n, Bilbao, Spain*

□ *In this study, the commercial finite element software FORGE2005®, able to solve complex thermo-mechanical problems is used to model titanium alloy dry machining. One of the main machining characteristics of titanium alloys is to produce a special chip morphology named "saw-tooth chip" or serrated chip for a wide range of cutting speeds and feeds. The mechanism of saw-tooth chip formation is still not completely understood. Among the two theories about its formation, this study assumes that chip segmentation is only induced by adiabatic shear band formation and thus no material failure occurs in the primary shear zone. Based on the assumption of material strain softening, a new material law was developed. The aim of this study is to analyze the newly developed model's capacity to correctly simulate the machining process. The model validation is based on the comparison of experimental and simulated results, such as chip formation, global chip morphology, cutting forces and geometrical chip characteristics. A good correlation was found between the experimental and numerical results, especially for cutting speeds generating low tool wear.*

Keywords chip segmentation, finite element method, machining, strain softening

1. INTRODUCTION

Titanium alloys show attractive characteristics with respect to their (a) density (60% that of a typical steel), (b) mechanical characteristics (quite high until 600°C), and (c) good corrosion resistance. These outstanding properties allow their use in the aeronautical industry, where the material is subjected to extreme loads. The aeronautics and aerospace fields are their first historical applications because 80% of the

Address correspondence to Madalina Calamaz, Laboratoire Matériaux Endommagement Fiabilité Ingénierie des Procédés (LAMEFIP), Arts et Métiers ParisTech, CER de Bordeaux, Esplanade des Arts et Métiers, Talence 33405, France. E-mail: Madalina.CALAMAZ@ENSAM.EU

titanium alloys have been utilized for these applications. Today, titanium represents 6 to 9% of the aircraft mass. Parts used in these areas must have a high dimensional accuracy and good surface quality, which is achieved by a machining operation. However, titanium alloys are difficult to machine, mainly because of their poor thermal properties leading to high temperatures at the tool-chip interface and rapid cutting tool wear. The high chemical reactivity with many tool materials and the weak elastic modulus, which generates harmful vibrations for the tool-workpiece structure, also contribute to the low machinability of this aeronautical material.

It is well known that temperature, together with normal stress generated at the tool/chip interface, are critical parameters for the tool wear and the workpiece material damage. Despite their great importance on tool life, these parameters are not well understood because they are very difficult to access through experimentation. To overcome these experimental limits, significant effort has been devoted to the development of computational models of high-speed machining. The machining numerical simulation enables these parameters and their evolution with respect to the cutting conditions to be estimated.

The choice of the material constitutive and tool-chip friction laws is of primary importance for the accuracy of the machining process simulation. The law usually used to describe the workpiece material behavior is based on the Johnson–Cook model. This law takes into account the strain and the strain rate hardening as well as the thermal softening effects. It expresses rather well the material behavior up to strain rates of $10^3\,s^{-1}$ and strain of 0.3. However, the level of strain and strain rates in machining process is much higher (strains higher than 1 and strain rates up to $10^5\,s^{-1}$). When machining titanium alloys, serrated chips are obtained at relatively low cutting speeds and feeds. In a previous work (Calamaz et al., 2008), it was shown that the use of the Johnson–Cook material model in simulation leads to a continuous chip, different from the segmented one observed experimentally.

Some authors consider that saw-tooth chip formation is due to a thermoplastic instability, while others explain this phenomenon by considering initiation and propagation of cracks inside the primary shear zone of the workpiece material.

Shaw et al. (1954) and Komanduri and Turkovich (1981) consider that this kind of chip morphology is due to a plastic instability occurring during the cutting process. This phenomenon would result from a competition between thermal softening and work hardening in the primary shear zone.

In most cases, the simulation of serrated chip is possible through the implementation of a failure model in the numerical machining simulation. The Johnson–Cook (Arrazola et al., 2006; Barge et al., 2005; Li and He, 2006; Pantalé et al., 2004), Latham and Cockroft (Ceretti et al., 1999;

Hua and Shivpuri, 2004; Umbrello, 2008), Brozzo's (Umbrello et al., 2004) damage models, etc., are some criteria used to simulate the crack initiation and propagation into the primary shear zone during the chip formation. For example, Brozzo's criterion takes into account the effect of hydrostatic stress on the chip segmentation during orthogonal cutting (Umbrello et al., 2004).

In the study of Obikawa and Usui (1996), when the plastic strain in a mesh node reaches a critical predefined value, this element is removed, indicating the initiation of a crack within the primary shear band. Marusich and Ortiz (1995) consider that damage happens when a critical stress depending on the material toughness is reached. Guo et al. (2006) used the Baumann–Chiesa–Johnson material law and a cumulative damage model to simulate serrated chip formation during the cutting of the AISI 52100 steel. In their work, it is not clear whether the serrated morphology results from the plastic flow according to the used material law or is a consequence of the damage criterion, giving rise to damaged finite element removal.

Baker et al. (2002) studied the numerical simulation of serrated chips without making any comparison with experimental chips. For the Ti-6Al-4V, they use equivalent stress-strain curves showing strain softening phenomenon. No damage criterion is introduced in the simulations and the segmented chip results from a localization of the plastic strain. This study does not propose any mathematical formulation for the material behavior law.

During machining, the workpiece material is subjected to high strain and temperature levels which may generate microstructure transformations, such as dynamic recovery and/or recrystallisation. This type of microstructure evolution during deformation at high temperature often leads to a stress-strain curve showing a strain-softening phenomenon. This strain-softening phenomenon is characterized by stress-strain curves showing strain hardening followed by a decrease of stress after a given strain.

This strain softening phenomenon was identified by carrying out torsion tests at high temperature on pure aluminum (Kassner et al., 2002) and on different Al–Mg–Si alloys (Pettersen and Nes, 1954). Kassner et al. (2002) confirm that for pure aluminum, the peak stress is reached at strains less than 0.5. Increasing the strain further leads to a gradual material softening. Then, the stress reaches a nearly constant level, becoming independent of strain.

The dynamic recovery and/or recrystallization have been observed in Ti-6Al-4V titanium alloy microstructure after hot processing at temperatures beyond the β-transus temperature (Ding and Guo, 2004). According to Ding and Guo (2004), the dynamic recrystallization is more

pronounced when the material undergoes high strains, which is the case during the machining process.

Based on the assumption of strain softening phenomenon, a first formulation of the material law was developed by Calamaz et al. (2008). This first formulation had to be improved because, in this case, strain softening was observed at room temperature, whereas it should appear from about 0.3 times the melting temperature, as shown in experimental results of Doege et al. (1986). Despite this problem, the preliminary formulation (MJC), has undoubtedly improved the quality of the numerical machining predictions under cutting speeds where the Johnson–Cook law has shown its limits.

The purpose of this study is to analyze the newly developed model's capacity to correctly simulate the machining process for a wide range of cutting speeds. The criteria used to validate the numerical simulation are: (a) the chip formation, (b) the global chip morphology, (c) the cutting forces and (d) the geometrical characteristics of the chip, i.e., the segment width *Ls* (cutting length/number of segments), the maximum (h_1) and minimum (h_2) segment height. The parameter h_2 was measured on the experimental chip without taking into account the possible existence of cracks inside the shear bands because no damage criterion was introduced in the simulation.

The commercial finite element software FORGE 2005®, which is able to solve complex thermomechanical problems, is used in this study to simulate the Ti-6Al-4V dry machining.

The scanning electron microscope (SEM) analysis of tool surfaces after machining was also used to measure tool-chip contact length. This parameter is measured by considering the length of contact over the tool rake face. Experimental results showed that the feed force was greatly influenced by this parameter, so it is important to take it into account for experimental/numerical comparisons.

NUMERICAL AND EXPERIMENTAL APPROACHES

The new behavior law we have developed is expressed below. The flow stress is defined as a function of strain, strain rate and temperature by equation (1):

$$\underbrace{\sigma = (A + B \cdot \varepsilon^{n}) \cdot \left(1 + C \cdot \ln\left(\frac{\dot{\varepsilon}}{\dot{\varepsilon}_0}\right)\right) \cdot \left(1 - \left(\frac{T - T_r}{T_m - T_r}\right)^{m}\right)}_{\text{Johnson–Cook}} \underbrace{\cdot \left(D + (1 - D) \cdot \tanh\left(\frac{1}{\varepsilon + \varepsilon_0}\right)\right)}_{\text{S}} \quad (1)$$

This law will be called hereafter as TANH, from the tangent hyperbolic function introduced into this equation. With respect to the Johnson–Cook law, an additional term (S) modeling the strain softening has been added. The values of constants in the Johnson–Cook law (A, B, C, n, m) are obtained from Shivpuri and Hua (2001). $\dot{\varepsilon}_0$ represents the reference strain rate, Tr and Tm, the room and melting temperatures, respectively. The constant ε_0 can modulate the strain corresponding to the peak stress.

The strain softening phenomenon being dependent on the equivalent strain and temperature, the parameter D in equation (1) is function of these two variables:

$$D = 1 - \left(\frac{p \cdot \varepsilon}{1 + p \cdot \varepsilon} \cdot \tanh \left(\frac{T - T_r}{T_{\text{rec}} - T_r} \right)^q \right) \tag{2}$$

The constant p controls the slope of the stress-strain curve after the peak stress, T_{rec}, the onset temperature for the strain softening phenomenon, and q, the temperature range over which the strain softening phenomenon develops.

Figure 1 shows a comparison between the Johnson–Cook and TANH laws for different temperatures and a strain rate of $10^5\,\text{s}^{-1}$. The constant values are presented in Table 1. At room temperature (Figure 1), the flow stress is the same for both material laws. When the temperature rises to 225°C (Figure 1), the TANH flow stress is slightly lower than that given by the Johnson–Cook law, but there is still no appearance of strain softening, so the flow stress increases with strain.

For a temperature of 305°C (Figure 1) and a low strain, both laws are similar until a given strain level (0.7). Above this value, the Johnson–Cook

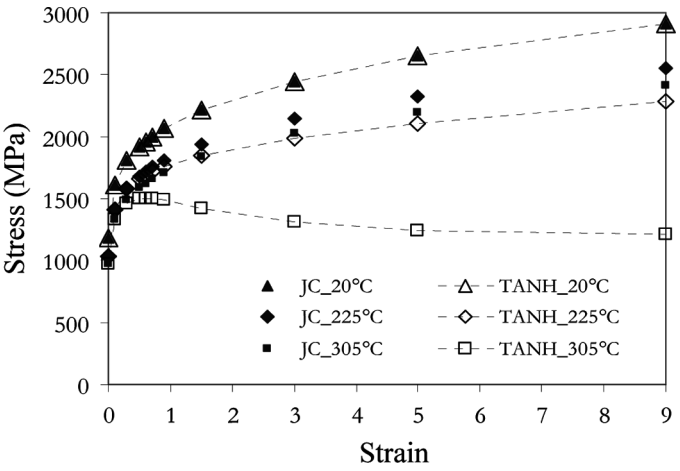

FIGURE 1 Equivalent stress-strain curves of Ti-6Al-4V for Johnson–Cook (JC) and TANH laws for different temperatures and a strain rate of $105\,\text{s}^{-1}$.

TABLE 1 Parameters Used for TANH and Johnson–Cook Laws (Shivpuri and Hua, 2001)

Behavior law	A (MPa)	B (MPa)	C	n	m	ε_0	p	T_{rec} (K)	r	q
TANH	870	990	0,011	0,25	1	0,7	0,6	600	1	5
JC	870	990	0,011	0,25	1	–	–	–	–	–

flow stress increases with strain while the TANH flow stress decreases until a quasi-stationary state. This type of macroscopic behavior corresponds to the appearance of the dynamic recovery/recrystallisation phenomena. For a higher temperature, the TANH flow stress evolves in the same way, but the stress decrease after the peak is more pronounced.

Creating a new material model by only considering an additional term to the Johnson–Cook (JC) law is interesting because the JC parameters are already identified for many materials. The number of parameters to be identified is thus reduced to those of the new term S. They are identified by inverse analysis based on the experimental cutting results for 60 m/min and 180 m/min cutting speed (the global chip morphology, the cutting forces and the geometrical characteristics of the chip, i.e., the segment width Ls – cutting length/number of segments –, the maximum (h_1) and minimum (h_2) segment heights). In other terms, machining simulations with different values of material law parameters (only the S term parameters; A, B, C, n and m are constant) were carried out and the predicted results were compared with the experimental ones. The combination of parameters which fitted better the experimental results (at these 2 speeds) has been chosen. For simulations with cutting speeds between 21 m/min and 235 m/min, the S term parameters are the same as those identified for the two cutting speeds (see Table 1).

The Ti-6Al-4V thermal properties depend on temperature. The specific heat increases linearly from 565 J/KgK at room temperature to 1060 J/KgK at 980°C. The thermal conductivity also increases linearly from 6.6 W/mK at 20°C to 21.5 W/mK at 1050°C. The coefficient of thermal expansion is slowly modified with temperature (between 9.4e-006 K^{-1} at room temperature and 1.07e-005 K^{-1} at 1000°C).

The contact at the tool-chip interface is modeled by a Coulomb friction law with a constant friction coefficient (0.3) for all simulations. The heat generated by friction at the tool/chip interface is dissipated inside these two bodies according to their respective effusivities. Thermal exchanges are considered between (a) the tool and the workpiece through a heat exchange coefficient h_{tw} and (b) the workpiece and the environment through another exchange coefficient h_{we}.

FORGE2005 is based on a mixed velocity-pressure formulation and the discretization of the workpiece is performed using the so-called

Mini-element ($P1+/P1$). It is based on linear isoparametric triangle and a bubble function is added at the element level in order to satisfy the Brezzi/Babuska condition (Brezzi and Fortin, 1991). An automatic remeshing procedure, based on mesh topology improvement (Gruau and Coupez, 2003), is used to avoid excessive element distortion induced by the cutting process.

The FORGE2005® software allows the definition of areas with a refined mesh. A preliminary mesh sensitivity study was done and the results have shown that mesh sizes lower than 2 μm do not affect much (differences less than 9%) the simulation results in terms of chip segmentation, temperature, etc. Thus, a 2 μm size mesh was used around the primary and secondary shear zones to detect strain localization (Figure 2).

The tool discretization would also increase the size of the problem and therefore the computation time. Therefore, the simulations are often carried out by considering a rigid tool to which the cutting speed *Vc* is imposed. In the present study, this approach has also been followed. In all simulations, the cutting length is fixed to 1 mm to reduce the computation time.

The experimental turning tests were carried out in orthogonal cutting configuration. In this configuration, the workpiece is a Ti-6Al-4V billet and it is prepared by making grooves. The tool material is tungsten carbide and its geometry is defined by a rake angle of 0°, a clearance angle of 11° and an edge radius of 20 μm. The experimental and simulated cutting conditions considered in this study are: (a) cutting speeds between 21 m/min and 235 m/min and, (b) a feed of 0.1 mm/rev.

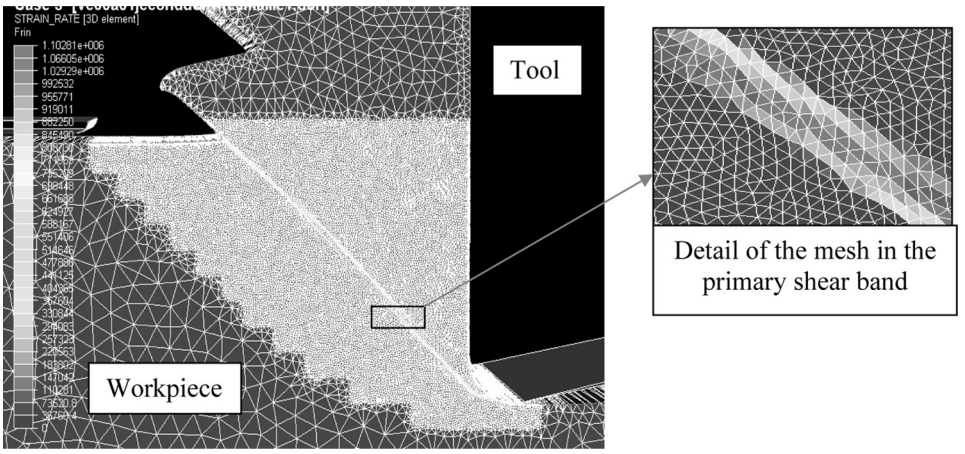

FIGURE 2 Example of workpiece mesh during the chip formation.

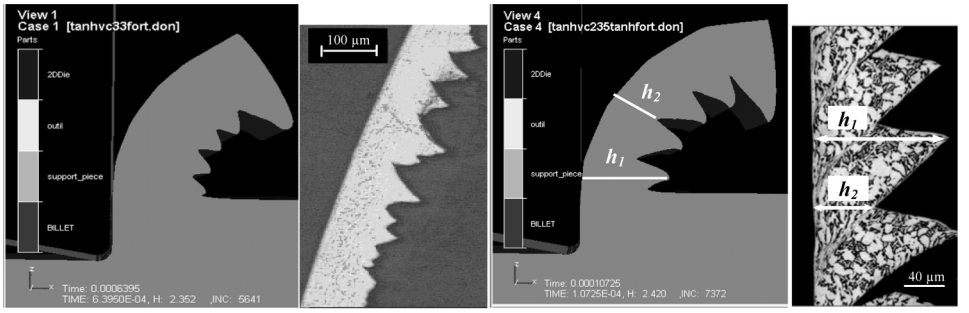

(a) (b) (c) (d)

FIGURE 3 Numerically simulated (a, c) and experimentally observed (b, d) chips obtained for machining with a cutting speed of 33 m/min (a, b) and 235 m/min (c, d); (feed: 0.1 mm/rev).

RESULTS AND DISCUSSION

Experimental and Predicted Chip Morphology

Figure 3 shows the experimentally observed and numerically simulated chips obtained at low and high cutting speeds. It can be seen that the global morphology of the predicted chip is similar to the experimental one for both low and high cutting speeds.

Figure 4(a) shows a comparison between the maximum segment height (h_1) of predicted and experimental chips. A good correlation is obtained over the range of cutting speeds studied. The most difficult chip parameter to predict by numerical simulations is the minimum segment height (h_2). For cutting speeds of 75 m/min and 94 m/min this parameter is overestimated, but a very good correlation is obtained for higher cutting speeds (Figure 4(b)).

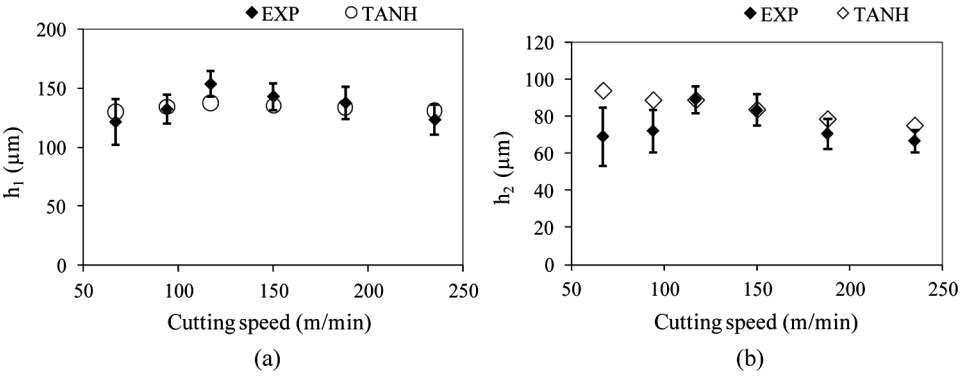

FIGURE 4 Comparison between the characteristics of experimental (EXP) and predicted (TANH) chips for different cutting speeds.

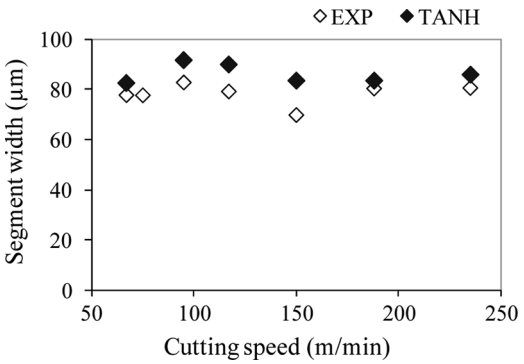

FIGURE 5 Comparison between the segment average width of experimental (EXP) and predicted (TANH) chips for different cutting speeds.

The segment average width (*Ls*) of numerically simulated chips is also in accordance with experiments (Figure 5) for all the cutting speeds studied. Therefore, the use of the TANH law improves significantly the estimation of geometrical chip parameters for all simulated cutting conditions, which is not the case when using the Johnson–Cook law (Calamaz et al., 2008). During machining, the use of a high-speed CCD camera allows the visualization of the different stages of a chip formation. Figure 6 shows a comparison between experimentally observed and numerically simulated chip formation.

For both experimental and numerical chips, the same stages of segment formation can be distinguished: (a) beginning of strain localization along a curved shear band (Figure 6(a)), (b) shearing in the primary shear band (Figure 6(b)), and, (c) curvature change of the primary shear band (Figure 6(c)).

Experimental and Numerical Cutting Forces and Contact Length

Figure 7 shows a comparison between the measured and predicted cutting forces for different cutting speeds. The cutting force predicted for low speeds (33 m/min and 67 m/min) is very close to the experimental value. For higher cutting speeds, the cutting force is slightly underestimated but the correlation is still acceptable.

The model also predicts a slight decrease of the cutting force when the cutting speed increases, which is not clearly showed by the experimental results. The trend predicted by the model reflects the temperature increase in the primary shear band leading to a lower flow stress and therefore a lower cutting force. Experimentally, the tool wear, which is more pronounced when the cutting speed increases, might change the conditions at the tool/chip interface and, therefore, more or less hide this effect.

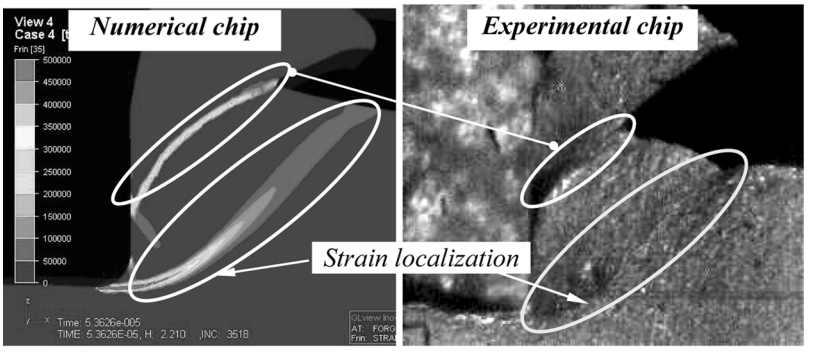

(a)

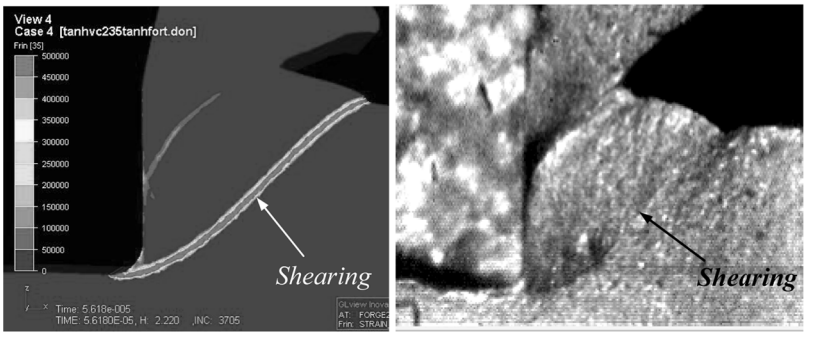

(b)

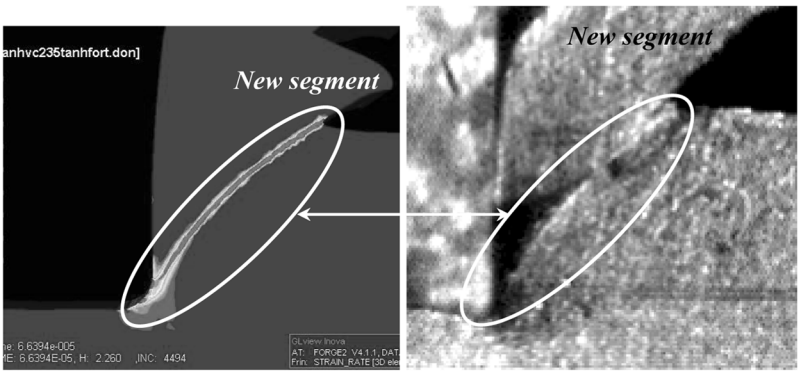

(c)

FIGURE 6 Stages of a numerical and experimental segmented chip formation: (a) beginning of strain localization along a concave shear band, (b) shearing in the primary shear band, and (c) change of the curvature of the primary shear band.

In Figure 8, the predicted feed force is compared with the experimental one for different cutting speeds. For low cutting speeds, the correlation is very good. However, for cutting speeds exceeding 94 m/min, there is a great difference between the predicted and experimental feed forces.

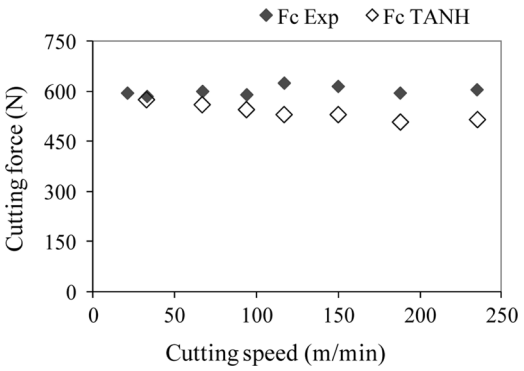

FIGURE 7 Comparison between experimental (EXP) and predicted (TANH) cutting forces (Fc) for different cutting speeds.

Experimental results showed that the feed force is influenced by the tool-chip contact length and by the tool wear. The contact length predicted by the simulation is underestimated, and the mismatch is very important for speeds exceeding 94 m/min (Figure 9). In numerical simulation, the tool-chip contact conditions are unchanged for all cutting speeds since the friction coefficient is constant and no tool wear is considered. Experimentally, these interface conditions evolve with the cutting speed. In the studies of Haglund et al. (2008) and Filice et al. (2007), the authors used different friction models to simulate the friction conditions at the tool-chip interface. In both cases, the contact length is greatly underestimated, regardless of the friction law used. Therefore, the friction law is not considered to be the main reason for the mismatch between predicted and observed tool-chip contact lengths.

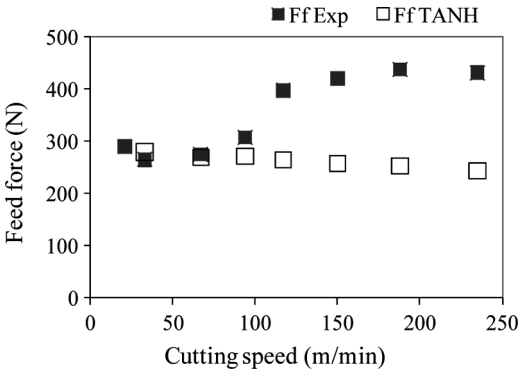

FIGURE 8 Comparison between experimental (EXP) and predicted (TANH) feed forces (Ff) for different cutting speeds.

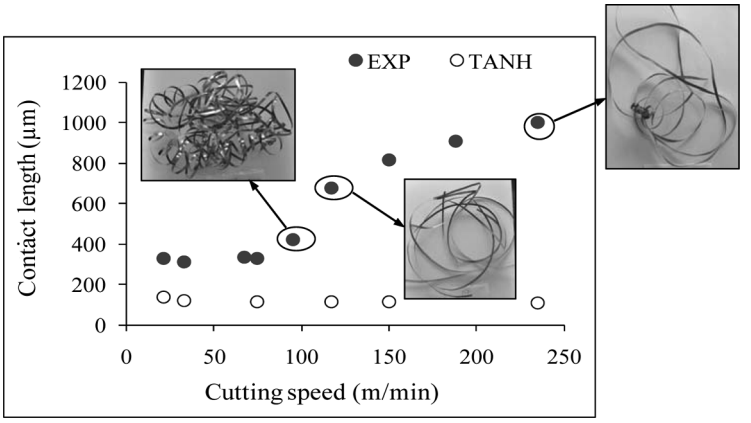

FIGURE 9 Comparison between experimentally observed (EXP) and numerically predicted (TANH) tool-chip contact lengths for different cutting speeds.

The increase of tool wear with increasing cutting speed may generate a local change of the tool geometry and thus a modification of the chip flow. This mesoscopic phenomenon would induce, at a macroscopic scale, a modification of the chip rolling, as shown in Figure 9. Because the tool wear is not taken into account in the simulation, it is not surprising to observe a mismatch between numerical and experimental feed forces. Despite differences in terms of feed force and contact length, this new constitutive law offers great improvements when compared with actual results in bibliography.

CONCLUSIONS

Taking into account the possibility of a strain softening phenomenon occurring from a given temperature and deformation level, the TANH law improves significantly the quality of the predictive model, particularly regarding the chip morphology. The new constitutive law is able to correctly predict the chip formation, chip morphology and to give a good estimation of the chip characteristics over a quite large range of cutting speeds.

Predicted cutting and feed forces are similar to those recorded experimentally for low cutting speeds, i.e., when the tool wear remains low. Simulations taking into account the tool wear at high cutting speeds might give higher feed forces, closer to those recorded experimentally. Experimental results showed that the feed force evolution is related to the modification of the contact length. In this study, the interface tool-chip conditions are simply described by a Coulomb friction law. The use of a more adaptive friction model at the same time with a tool wear model

might give rise to a better correlation between experimental and predicted contact length, and hence also feed force, at high cutting speeds.

Based on the assumption of any softening phenomenon, such as dynamic recovery and/or recrystallisation for example, a new effective model was developed showing a good correlation between predictions and experimental results over a wide range of cutting speeds.

However, it should be stated that the Johnson–Cook and a damage law should be able to give adequate predictions by fitting the damage parameter.

REFERENCES

Arrazola, P.J.; Ugarte, D.; Villar, J.A.; Marya, S. (2006) Finite element modelling: a qualitative tool to study high speed machining. *Proceedings of Fifth International Conference on High Sped Machining (HSM)* March 14–16, Metz, France, pp. 239–246.

Barge, M.; Hamdi, H.; Rech, J.; Bergheau, J.-M. (2005) Numerical modelling of orthogonal cutting: influence of numerical parameters. *Journal of Materials Processing Technology*, 164–165: 1148–1153.

Baker, M.; Rosler, J.; Siemers, C. (2002) A finite element model of high speed metal cutting with adiabatic shearing. *Computers and Structures*, 80(5–6): 495–513.

Brezzi, F.; Fortin, M. (1991) *Mixed and Hybrid Finite Element Methods*. Springer-Verlarg, New-York, Berlin-Heidelberg.

Calamaz, M.; Coupard, D.; Girot, F. (2008) A new material model for 2D numerical simulation of serrated chip formation when machining titanium alloy Ti-6Al-4V. *International Journal of Machine Tools & Manufacture*, 48: 275–288.

Ceretti, E.; Lucchi, M.; Altan, T. (1999) FEM simulation of orthogonal cutting: serrated chip formation. *Journal of Materials Processing Technology*, 95: 17–26.

Ding, R.; Guo, Z.X. (2004) Microstructural evolution of a Ti-6Al-4V alloy during β-phase processing: experimental and simulative investigations. *Materials Science and Engineering A*, 365: 172–179.

Doege, E.; Meyer-Nnolkemper, H.; Saeed, I. (1986) *Fliebkurven-Atlas metallischer Werkstoffe*. Munich; Vienna, Hanser Verlag.

Filice, L.; Micari, F.; Rizzuti, S.; Umbrello, D. (2007) A critical analysis on the friction modelling in orthogonal machining. *International Journal of Machine Tools & Manufacture*, 47: 709–714.

Guo, Y.B.; Wen, Q.; Woodbury, K.A. (2006) Dynamic material behavior modelling using internal state variable plasticity and its application in hard machining simulations. *Journal of Manufacturing Science and Engineering*, 128: 749–756.

Gruau, C.; Coupez, T. (2003) Anisotropic and multidomain mesh automatic generation for viscous flow finite element method. In: *International Conference on Adaptive and Modeling Simulation (ADMOS 03)* Goteburg.

Hua, J.; Shivpuri, R. (2004) Prediction of chip morphology and segmentation during the machining of titanium alloys. *Journal of Materials Processing Technology*, 150: 124–133.

Haglund, A.J.; Kishawy, H.A.; Rogers, R.J. (2008) An exploration of friction models for the chip–tool interface using an Arbitrary Lagrangian–Eulerian finite element model. *Wear*, 265: 452–460.

Kassner, M.E.; Wang, M.Z.; Perez-Prado, M.-T.; Alhajeri, S. (2002) Large-strain softening of aluminium in shear at elevated temperature. *Metallurgical and Materials Transactions A*, 33: 3145–3153.

Komanduri, R.; Turkovich, B.F. (1981) New observations on the mechanism of chip formation when machining titanium alloys. *Wear*, 69: 179–188.

Li, L.; He, N. (2006) A FEA study on mechanisms of saw-tooth chip deformation in high speed cutting of Ti-6-Al-4V alloy. *Fifth International Conference on High Speed Machining (HSM)* March 14–16, Metz, France, pp. 759–767.

Marusich, T.D.; Ortiz, M. (1995) Modelling and simulation of high-speed machining. *International Journal for Numerical Methods in Engineering*, 38(21): 3675–3694.

Obikawa, T.; Usui, E. (1996) Computational machining of titanium alloy-Finite element modelling and a few results. *Transactions of the ASME*, 118: 208–215.

Pantalé, O.; Bacaria, J.-L.; Dalverny, O.; Rokotomalala, R.; Caperaa, S. (2004) 2D and 3D numerical models of metal cutting with damage effects. *Computer Methods in Applied Mechanics and Engineering*, 193: 4383–4399.

Pettersen, T.; Nes, E. (1954) On the origin of strain softening during deformation of aluminium in torsion to large strains. *Metallurgical and Materials Transactions A*, 34: 2727–2736.

Shaw, M.C.; Dirke, S.O.; Smith, P.A.; Cook, N.H.; Loewen, E.G.; Yang, C.T. (1954) Machining titanium. *Massachusetts Institute of Technology Report* to U.S. Air Force.

Shivpuri, R.; Hua, J. (2001) Microstructure-mechanics interactions in modelling chip segmentation during titanium machining. *Annals of the CIRP*, 51: 85–89.

Umbrello, D. (2008) Finite element simulation of conventional and high speed machining of Ti-6Al-4V alloy. *Journal of Materials Processing Technology*, 196(1–3): 79–87.

Umbrello, D.; Hua, J.; Shivpuri, R. (2004) Hardness-based flow stress and fracture models for numerical simulations of hard machining AISI 521000 bearing steel. *Materials Science and Engineering A*, 374: 90–100.